Extended Work Function Shift of Large-Area Biofunctionalized Surfaces Triggered by a Few Single-Molecule Affinity Binding Events

Cinzia Di Franco, Eleonora Macchia, Lucia Sarcina, Nicoletta Ditaranto, Aniqa Khaliq, Luisa Torsi,* and Gaetano Scamarcio*

Few binding events are here shown to elicit an extended work function change in a large-area Au-surface biofunctionalized with $\approx 10^8$ capturing antibodies. This is demonstrated by Kelvin probe force microscopy (KPFM), imaging a $\approx 10^5$ μm^2 wide Au-electrodes covered by a dense layer ($\approx 10^4$ μm^{-2}) of physisorbed anti-immunoglobulin-M (anti-IgM). A 10 min incubation in 100 μL phosphate buffer saline solution encompassing ≈ 10 IgM antigens (10^{-19} mole L$^{-1} \equiv 10^2 \times 10^{-21}$ M) produces a work function shift $\Delta W \approx -60$ meV. KPFM images prove that this shift involves the whole inspected area. Notably, no work function change occurs upon incubation in highly concentrated (3×10^{-15} M) nonbinding IgG solutions. The ΔW measured by KPFM is in quantitative agreement with the threshold voltage shift of an electrolyte-gated single-molecule large-area transistor (SiMoT). The findings provide direct experimental evidence for the SiMoT ultrahigh sensitivity, by imaging the extensive shift of the gate work function, likely arising from collective surface phenomena, elicited by single-molecule binding events.

1. Introduction

The work function (W) is a key physical quantity that controls phenomena involving the extraction of electrons from a material, e.g., thermionic emission, photoelectron emission, and contact potential difference at the interface between two conducting materials.[1] Defined in metals as the energy difference between the vacuum level in the proximity of the surface (E_V) and the Fermi energy (E_F), W is also conveniently expressed as $W = e\Phi_B + e\Phi_S$, i.e., the sum of a bulk potential energy term $e\Phi_B = E_{V,\infty} - E_F$ and a surface potential energy term $e\Phi_S = E_V - E_{V,\infty}$, where $E_{V,\infty}$ and E_V are the vacuum levels at an infinite distance from the surface and in close proximity with the surface, respectively (**Figure 1**). An intrinsic contribution to the surface term arises from the discontinuity of the crystal potential at the surface, where a layer of dipoles with negative charges oriented toward the vacuum side exists. The surface potential term is strongly influenced by the presence of surface adsorbates. As an instance, the biofunctionalization of a metal surface with a self-assembled monolayer of recognition elements, e.g., a dense layer of antibodies, can change the surface potential. A further change can be induced locally by the interaction with ligands (e.g., affinity antigens).

The above-mentioned effects, at the basis of the ultrahigh sensitivity of electrolyte-gated single-molecule large-area transistors (SiMoT),[2,3] arises from W changes elicited by an affinity-binding event occurring at a millimeter-wide gate bio-functionalized with trillions of capturing antibodies. The resulting threshold voltage shift (ΔV_T) modulates the transistor-channel conductance and generates a detectable response, indirectly related to the W shift. In Figure 1 a sketch of the energy diagram evidencing the surface potential shift $\Delta\Phi_S$ and the corresponding threshold voltage shift ΔV_T upon binding, is given.

The main goal of the present work is to directly measure the surface potential changes associated with antigen–antibody bindings at a large-area biofunctionalized metal surface.

Kelvin probe force microscopy is a suitable technique to measure the contact potential difference between a scanning probe metallic tip and a sample surface, a quantity that

C. Di Franco, A. Khaliq, G. Scamarcio
CNR
Istituto di Fotonica e Nanotecnologie c/o Dipartimento Interateneo di Fisica
Università degli Studi di Bari Aldo Moro
Bari 70125, Italy
E-mail: gaetano.scamarcio@uniba.it
C. Di Franco, E. Macchia, L. Sarcina, N. Ditaranto, A. Khaliq, L. Torsi
Dipartimento di Chimica
Università degli Studi di Bari Aldo Moro
Bari 70125, Italy
E-mail: luisa.torsi@uniba.it
A. Khaliq, G. Scamarcio
Dipartimento Interateneo di Fisica
Università degli Studi di Bari Aldo Moro
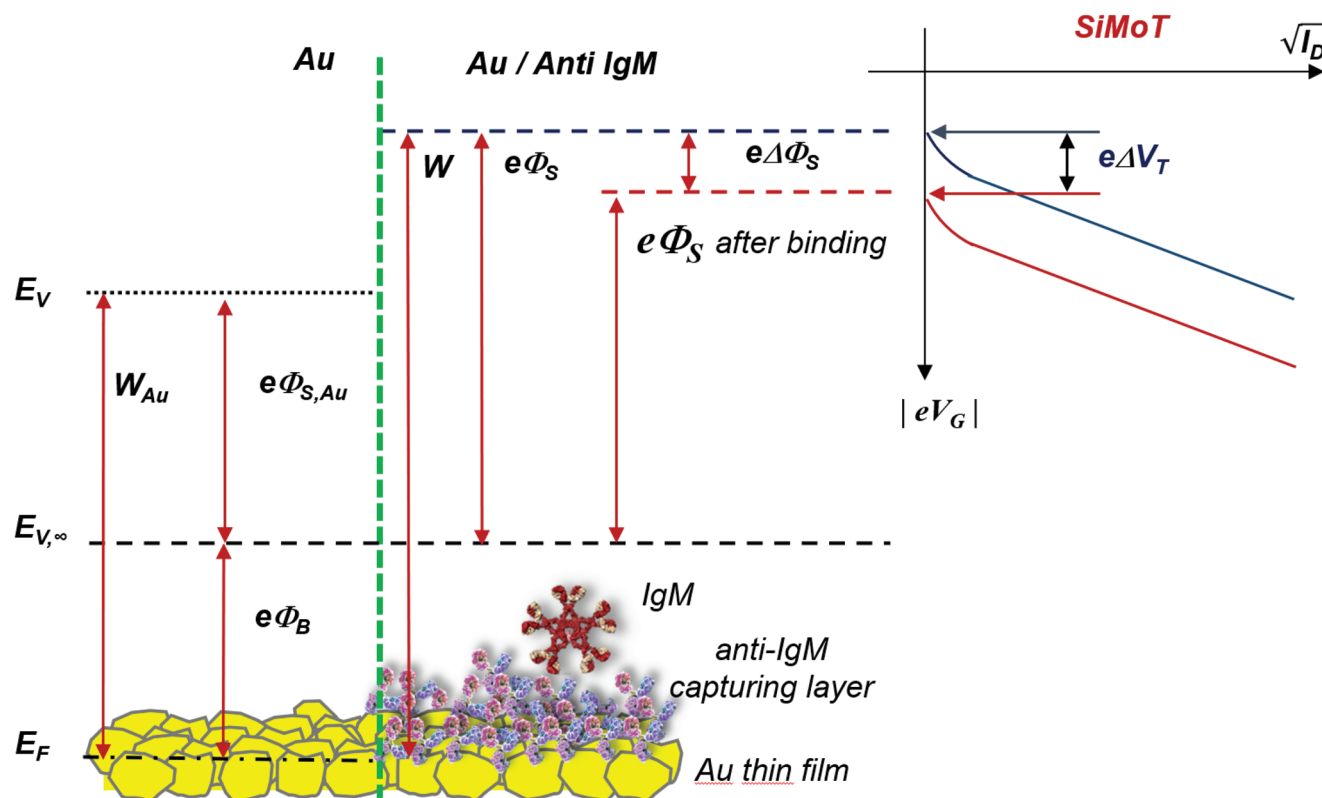Bari 70125, Italy

Figure 1. Surface potential shift in an Au/anti-IgM interface before and after single-molecule binding. Schematic cross-sectional view of the interface between bare and physisorbed anti-Immunoglobulin (anti-IgM) biofunctionalized Au surfaces, along with the work function (W), and the surface potential energy ($e\Phi_S$) before and after IgM single-molecule binding. The surface potential shift ($\Delta\Phi_S$) is directly assessed by Kelvin probe force microscopy (KPFM). The electrolyte-gated single-molecule large-area transistor (SiMoT) assesses the threshold voltage shift ($e\Delta V_T = e\Delta\Phi_S$) induced by the single-molecule binding.

is closely related to the Φ_S spatial distribution.[4,5] Notably, the transfer characteristics and the relevant extracted threshold voltages of an organic field-effect transistor, have been also proven to shift in the presence of a dipole at the gating interface.[6–8] Here, we use a combination of atomic force microscopy (AFM) and KPFM to directly measure the surface potential shift $\Delta\Phi_S$ of biofunctionalized Au/anti-IgM interfaces upon affinity single-molecule binding events. We further correlate $\Delta\Phi_S$ with the indirectly assessed shift of the SiMoT ΔV_T, both involving a change of W. The KPFM images further enable to assess the extent of the sample area involved in the single-molecule surface potential shift. This approach provides fundamental insights into the phenomenon of electrostatic changes induced by a few single-molecule binding events eliciting the shift of the surface potential of 10^8 capturing antibodies populating an area as large as 10^5 μm^2 supporting the hypothesis of the existence of surface amplification processes.

2. Results and Discussion

In an atomic force microscope operated in the Kelvin probe mode, local variations in the contact potential difference can be measured by applying a constant voltage between the oscillating AFM tip and the sample, to compensate for the electrostatic force originated by the contact potential difference itself. Feedback loop electronics enable such compensating voltage to correspond to the local surface potential to be measured (Note S1,

Supporting Information). A known problem for the extraction of quantitative values from KPFM images is the need for a reference standard constantly accessible during each scan. Typically, either a portion of the sample surface or the tip itself are taken as calibration standards.[9] This choice is critical as the KPFM measurements can be deeply affected by experimental parameters, e.g., tip-sample distance, potential applied to the tip, or experimental conditions, e.g., relative ambient humidity, and contamination by adventitious carbon.[10,11] The latter issue plagues also inert metals such as Au and causes time-dependent not monotonic work function changes as large as 0.5 V ($\approx$10%) upon exposure to ambient air.[11] To minimize the influence of the above extrinsic phenomena and enhance the reliability of the surface potential values extracted by KPFM we have adopted an experimental approach based on: i) the fabrication of patterned samples in which a biofunctionalized area with a typical size of 100–200 μm^2 is separated by a pristine Au area by a sharp interface (Note S2, Supporting Information); ii) the accurate choice of the experimental parameters (Note S3, Supporting Information), and iii) the simultaneous surface potential measurement of both the bare and the anti-IgM biofunctionalized Au areas (Au/anti-IgM) in each KPFM image (see Experimental Section). Meaningfully, we have demonstrated that while the surface potential values in selected areas may vary as a function of extrinsic parameters, the average value of the relative contact potential differences between the biofunctionalized and Au areas is largely insensitive to the external conditions (Note S3, Supporting Information). As
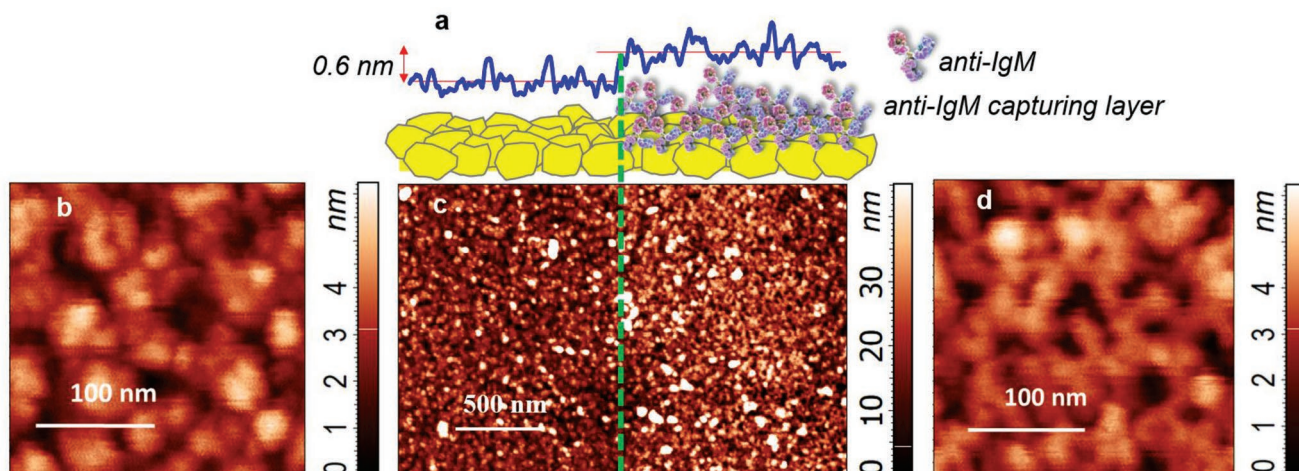
Figure 2. AFM images of the patterned Au/anti-IgM electrode. a) Schematic cross-sectional view of the interface between bare and physisorbed anti-IgM biofunctionalized Au surfaces. The blue line is the average profile. The measured height across the sharp interface is also shown. b) Topographic semi-contact AFM images of the pristine Au surface. c) Interface between the pristine Au (leftmost part) and the Au biofunctionalized (rightmost part) surfaces. d) the anti-IgM biofunctionalized Au surface. The green dashed line across panels a and c, marks the sharp interface.

a result, the surface potential difference $\text{SPD} \equiv \Phi_S - \Phi_{S,Au}$ is practically artifact-free and extremely sensitive to surface modification induced by affinity binding events, too.

Figure 2 shows the topographical AFM images acquired at the interface between the bare (leftmost) and the physisorbed anti-IgM covered (rightmost) areas of an Au-gate surface (see Note S4, Supporting Information for details). In the pictorial view of the Au/anti-IgM interface (Figure 1a) the measured AFM profile across the very sharp interface is also given showing a 0.6 nm increase in average heights at the edge with the anti-IgM capturing layer. This is compatible with a layer of antibodies lying mostly flat on the electrode surface. The bare Au image (Figure 2b) features quasi-spherical clusters 20–30 nm wide with a root mean square (rms) roughness of ≈0.9 nm, as expected for an e-beam evaporated gold thin-films.[12] Figure 2c shows the AFM image of the interfacial area, evidencing the morphological differences. The surface of the anti-IgM layer (Figure 2d) is characterized by a network of segments or chains, and a rms roughness of ≈1.3 nm. This is compatible with the presence of a dense physisorbed monolayer of anti-IgM molecules (≈10^{12} anti-IgM cm^{-2} or equivalently ≈ 10^9 anti-IgM on 10^5 μm^2—see Experimental Section), as demonstrated by surface plasmon resonance (SPR) data (Notes S5 and S6, Supporting Information).[2,13]

Figure 3 features the KPFM images (central panels) and the surface potential difference (SPD) histograms (panels on the right) of an Au/anti-IgM patterned electrode inspected before and after the occurrence of a few single-binding events. The panels on the left (Figure 3a,d,g,l) offer a pictorial view of each experiment performed. In the first row, results related to the pristine Au/anti-IgM sample are shown. The other rows are relevant to the Au/anti-IgM sample exposed to the non-binding Immunoglobulins G (IgGs) and the binding IgMs. Phosphate buffer saline (PBS, pH = 7.4, ionic strength = 162×10^{-3} M) solutions of the elicited antigens are assayed, to mimic physiological conditions. Specifically, Figure 3b,c shows the KPFM and the average SPD values measured across the pristine Au/anti-IgM interface, being 176 ± 20 mV.

This is taken as the baseline SPD difference encompassing bare gold and pristine (nonexposed to any antigen solution) anti-IgM. Figure 3e,f shows the KPFM image and the SPD (167 ± 20 mV) comparable to those of the baseline, within error bars, measured when the Au/anti-IgM sample is incubated for 10 min in 100 μL of a 3×10^{-15} M IgG solution. As IgG does not bind to anti-IgM, this suitably serves as the negative control experiment.

The same Au/anti-IgM electrode is incubated in the binding IgM solutions, afterward. Strikingly, after incubation in 100×10^{-21} M, and 10×10^{-18} M IgM PBS solutions, the KPFM images (Figure 3h,m) change appreciably, and the SPD values (128 ± 20 mV for the 100×10^{-21} M and 116 ± 20 mV for the 10×10^{-18} M) decreases by $\Delta\text{SPD} = -48 \pm 20$ mV (100×10^{-21} M, Figure 3i) and $\Delta\text{SPD} = 60 \pm 20$ mV (10×10^{-18} M, Figure 3n), respectively, compared to the baseline. Very relevantly, The KPFM images prove that such a large shift involves the whole wide area of 90 μm × 90 μm covered by ≈6×10^7 anti-IgM capturing proteins (Note S5, Supporting Information). This occurs in spite of the exiguous maximum number of IgM antigens (≈10–10^3) present in the 100 μL incubation volume that, by diffusion, can encounter the large area covered by anti-IgMs.[14] These findings provide direct experimental evidence that few antigen–antibody binding events generate extended work function changes on large-area biofunctionalized Au surfaces.

In **Figure 4** the ΔSPD data discussed in Figure 3, measured on up to three different Au/anti-IgM samples, are plotted as a function of the IgM concentration. Error bars are taken as one standard deviation of the SPD dispersion in the inspected area. As it is clear already at 100×10^{-21} M (less than 10 IgM proteins in 100 μL) a sizeable SPD shift is seen, while no response is recorded when the electrode is exposed to a much higher concentrated IgM solution (3×10^{-15} M, ≈10^5 IgG in 100 μL). All the details of the KPFM data plotted in Figure 4a, can be found in Note S7 (Supporting Information). For the sake of comparison, the Au/anti-IgM gate electrodes, exposed to PBS solution of IgM (3×10^{-15} M) and IgG (100×10^{-21} M, 10×10^{-18} M and 100×10^{-18} M),
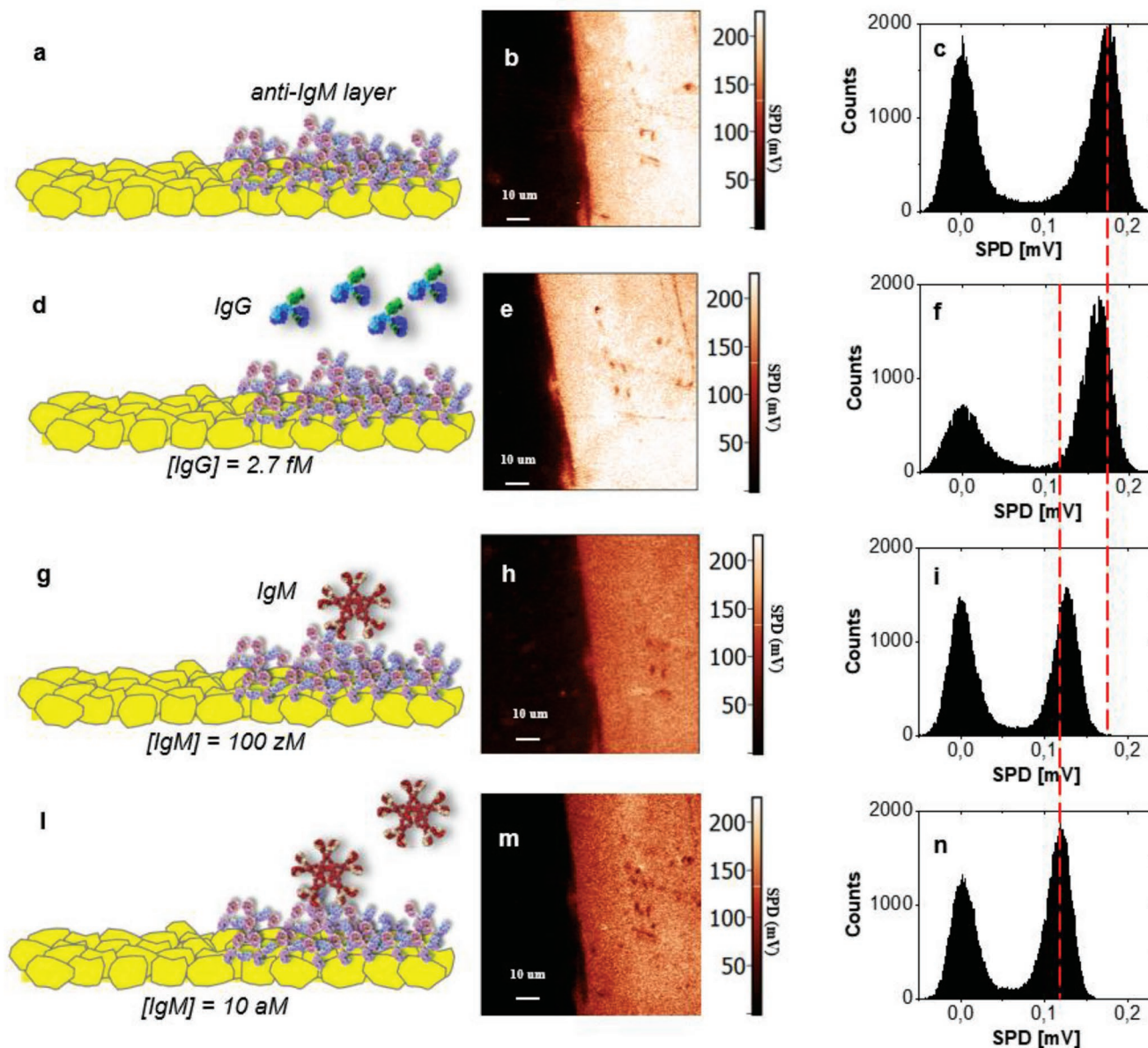
Figure 3. Surface potential changes induced by affinity binding events. a) Schematic cross-section and b) KPFM image of a 90 μm × 90 μm area close to the interface between the bare Au (leftmost) and the anti-IgM bio-functionalized Au (rightmost) surfaces. The physisorbed anti-IgMs act as capturing layer. c) Histogram of the surface potential values plotted as a function of the surface potential difference SPD between the local value of the contact potential difference and the SPD peak value of the bare Au. The sets of panes {d,e,f}, {g,h,i}, and {l,m,n} are similar to {a,b,c}, and show the cross-sections, KPFM images and SPD histograms of a sample sequentially incubated in a phosphate buffer saline (pH = 7.4, ionic strength = 162×10^{-3} M) solution of non-binding IgG at a concentration of 3×10^{-15} M (negative control), of IgM 100×10^{-21} M and IgM 10×10^{-18} M, as indicated in panes d, g, l, respectively.

are assessed with the SiMoT sensors.[2,3] In Figure 4b the SiMoT device structure is schematically shown along with typical transfer characteristics (Figure 4c) I_D–V_G (Note S8, Supporting Information), from which the threshold voltage change, ΔV_T, is extracted.[15,16] In Figure 4d the ΔV_T data (in triplicates), are shown.

The device structure in Figure 4b is that of an electrolyte-gated transistor in which the biofunctionalized gate is capacitively coupled to the channel, where charges are induced resulting in a measurable source–drain current I_D. When the gate work function changes due to the affinity binding, the

coupled charge double layers at the gate and channel interfaces adjust to compensate for the charge rearrangement. This reflects in the current changes (measured in Figure 4c) from which a threshold voltage shift can be extracted.

The comparison of the KPFM and the SiMoT homologous responses illustrates the striking correspondence between the threshold voltage shift $\Delta V_T \approx -60 \pm 30$ mV and the surface potential change $\Delta SPD \approx -60 \pm 20$ mV. This can be explained by considering the large gate area (5×10^7 μm²) as compared to the channel area (5×10^4 μm²) so no capacitive component is present in the measured value of V_T.

**ADVANCED
SCIENCE NEWS**

www.advancedsciencenews.com

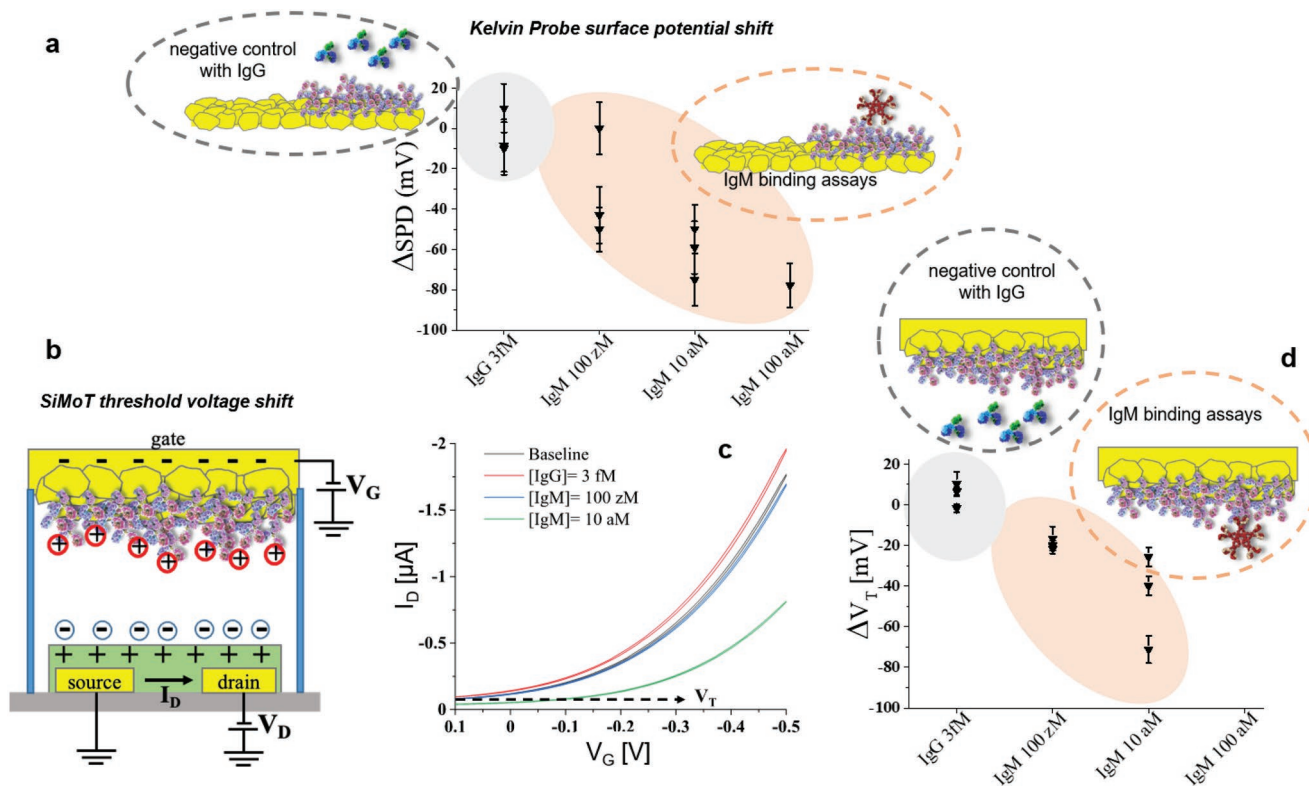**ADVANCED
MATERIALS
INTERFACES**

www.advmatinterfaces.de

Figure 4. Au/anti-IgM electrodes exposed to the same IgM concentrations show comparable responses in KPFM and SiMoT transducers. a) The SPD shift (ΔSPD) at different IgM concentrations as compared to the SPD measured on bare gold (reference). Au/anti-IgM electrodes are exposed to PBS solution of IgM (3×10^{-15} M) and IgG (100×10^{-21} M, 10×10^{-18} M and 100×10^{-18} M). b) Schematics of the electrolyte-gated SiMoT sensor device structure. The gate area is $\approx 5 \times 10^{-1}$ cm^2 while the density of anti-IgM is $\approx 2 \times 10^{12}$ cm^{-2}. c) Typical SiMoT transfer characteristics I_D versus V_G at $V_D = -0.4$ for the same samples as in panel (a). d) The plot of ΔV_T values extracted from the transfer transistor curves. Symbols and error bars show the mean and standard deviations over up to three replicates.

3. Conclusions

The SiMoT capability to detect a single protein in 100 µL was discovered in 2018[2] and demonstrated on a number of different sensing systems.[3,17–21] It was also demonstrated how a single antigen out of ten in 100 µL can reach by Brownian diffusion a millimeter wide surface in 10 min.[14] Recently, single-molecule reliable electronic detection was even proven possible with a capturing layer comprising trillions of barely physisorbed antibodies.[22] The SiMoT effect is striking as the footprint of a single protein ($\approx 10^{-4}$ µm^2) is 9 orders-of-magnitude smaller than the transducing large-area inspected by KPFM ($\approx 10^5$ µm^2). By the same token, a single IgM is detected at a surface that hosts trillions of capturing antibodies. Both these occurrences should result in single-binding events' signals being much lower than the noise level. In fact, this is not the case and the KPFM AFM data here shown, directly and clearly prove that the binding of less than 10 IgMs to an equal number of anti-IgMs shift the surface potential of 10^8 anti-IgMs that are highly packed on a 90×90 µm^2 wide gate. An amplification mechanism involving a domino-like propagation of the electrostatic (dipole) change triggered by the affinity binding at a single capturing antibody that eventually affects a multitude of other antibodies was postulated and modeled.[2] Previously it was assumed to be enabled by a collaborative effect involving

the dipoles of a hydrogen-bonding network associated with the antibodies' anchoring self-assembled monolayer.[2] But in fact, even a barely physisorbed layer works.[22] This implies that the electrostatic interactions among highly packed capturing antibodies segregated on the gate surface can enable the propagation of an electrostatic change occurring on one single capturing antibody. Indeed a long-range charge reorganization in concomitance with a conformational change during an affinity binding has been recently proven.[23] On the other hand, the mesogens (dipolar in nature) in a liquid crystal have been shown to propagate a reorientation of their structure for micrometers when an affinity binding involves a protein attached to the liquid crystal's surface.[24] This occurs via the reorientation of millions of mesogens molecules composing the liquid crystal film per protein bound. While differences are present with the SiMoT systems, there are similarities with the propagation of a dipolar electrostatic reorientation involving billions of dipoles (capturing antibodies) upon single-protein affinity binding.

4. Experimental Section

Materials: HPLC-grade water, hydrogen peroxide 30% (w/w), sulfuric acid 96%, anti-human immunoglobulin M (anti-IgM), human IgM ($\approx$950 kDa), IgG ($\approx$150 kDa), all purchased from Sigma–Aldrich, were

used with no further purification. Phosphate buffered saline (PBS, pH 7.4, ionic strength 162×10^{-3} M, Sigma-Aldrich-Merck KGaA) solution was prepared as described elsewhere.[2] All the immunoglobulins used are polyclonal antibodies.

Patterned Biofunctionalized Au Surfaces Fabrication: The samples were prepared from an n-doped silicon wafer with a thermally grown 300 nm thick SiO_2 layer on top. Before metal deposition, the wafer was sequentially cleaned via an ultrasonic bath in acetone, 2-propanol, and deionized water for 10 min, and then dried in a nitrogen flux. An adhesion promoter layer of titanium (thickness 5 nm) and then a gold layer (thickness 50 nm) were deposited by electron-beam evaporation with a rate of 0.1 Å s^{-1} at a pressure $<10^{-6}$ mTorr. The resulting gold-electrodes were cleaned from organic residues using a freshly prepared piranha solution, i.e., a mixture of sulfuric acid, water, and hydrogen peroxide, rinsed with HPLC-grade water, and dried in a nitrogen flux. The protocol of the gold gate biofunctionalization process is schematically depicted in Figure S1 (Supporting Information). To pattern the gold surface a mask shadows a portion of the gold electrode (Step 1), which is then dipped in a 0.1 mg mL^{-1} anti-IgM PBS solution for 150 min at 25 °C (Step 2). A physisorbed stable layer of capturing anti-IgM forms[22] on the free surface portion. The mask is removed afterward leaving the sharp Au/anti-IgM interface on the substrate (Step 3). The electrode is then extensively rinsed sequentially in PBS and in HPLC water and dried in air. Before the KPFM measurements, the patterned electrode is conditioned by immersing it in HPLC water along with a gold counter electrode and cycling is carried out by sweeping the potential in the $0.1 \div -0.5$ V range at scan rate of 100 mV s^{-1} for 20 cycles (step 4).

AFM and KPFM Measurements: The AFM and KPFM measurements were performed using a NT-MDT mod. Ntegra system and a platinum-iridium coated tip (PPP-EFM, Nanosensors) with apex size of 25 nm and resonance frequency $f \approx 69$ KHz. The SP images are obtained in the two-pass mode, consisting in the analysis of two sequential scans per line. During the first scan, the sample morphology is acquired in semi-contact mode. During the second scan, the tip is raised by a lift height LH = 250 nm and a DC+AC electrical signal is applied to the tip while the piezo scanner is off. The DC voltage, needed to nullify the tip oscillations, is a direct measure of the local SPD.[25] Areas of 90×90 μm^2 across the Au/anti-IgM interface were scanned. The KPFM images acquisition was performed by scanning the same area of the sample during the control and the sensing experiments to detect changes in the surface potential properties of the electrode after the highly specific IgM binding. During characterization, the topography and surface potential images were acquired simultaneously. All images have been processed with the Image Analysis software.

Single-Molecule KPFM Measurements Protocol: The anti-IgM biofunctionalized Au gate (steps 1 to 4) was immersed in the 100 µL PBS standard solution to be assayed for 10 min at room temperature (20–22 °C). The first experiment is the negative control carried out in a 3×10^{-15} M solution of the non-binding IgG. The electrode was washed thoroughly with HPLC deionized water and biased against the gold counter electrode and cycled, afterward, by sweeping the potential in the $0.1 \div -0.5$ V range for 20 cycles. After drying in air, the sample was measured with the KPFM. The same Au/anti-IgG electrode was immersed in 100 µL of a PBS standard solution with an IgM concentration of 100×10^{-21} M, 10×10^{-18} M and 100×10^{-18} M for 10 min. After each incubation, the electrode was washed and cycled, dried and assessed by KPFM.

Electrolyte-Gated SiMoT Fabrication and Single-Molecule Sensing: The SiMoT was fabricated starting from a silicon substrate, covered by a thermally grown SiO_2 layer. Source (S) and drain (D) interdigitated electrodes were photolithographically defined on a substrate, by electron-beam evaporated gold films (thickness 50 nm) on an adhesion layer of titanium (thickness 5 nm). The channel length is 5 µm and the geometrical channel width is 10^4 µm. A P3HT solution (2.6 mg mL^{-1} in chlorobenzene) filtered through a 0.2 µm mesh was spin-coated across and above the S and D electrodes, at 2×10^3 rpm for 20 s and annealed at 90 °C for 15 s. A polydimethylsiloxane well was glued around the interdigitated channels area and filled with 300 µL of deionized water (HPLC-grade), acting as the gating medium. This is addressed as the SiMoT measuring well. The transistor current-voltage transfer curves (source–drain current I_D versus V_G at $V_D = -0.4$ V) were acquired with a semiconductor parameter analyzer equipped with a probe station at RT. Before proceeding with the sensing measurements, the device was let to stabilize by resting in deionized water for about 12–24 h after deposition, according to a well-established protocol.[26] Afterwards, I_D was further stabilized by cycling the measurement of the transfer curve with clean bare gold gate in the $+0.1 \div -0.5$ V_G range, until the last three current traces overlapped. Usually from 10 to 20 cycles were needed. A functionalized gate was then incubated (at RT and in the dark) for 10 min in 100 µL of PBS. The functionalized gate was removed from the PBS solution, washed thoroughly with HPLC water, mounted in the SiMoT measuring well (exactly replacing the bare gold-gate previously used) and new transfer characteristics were registered. After the 10–20 cycles a stable I_0 baseline was measured and the same gate was immersed and incubated for 10 min in 100 µL of the PBS standard solutions of IgG at a concentration of 1×10^{-15} M (negative control experiment) and subsequently in standard solutions of IgM, with nominal concentrations of 100×10^{-21} M and 10×10^{-18} M. After incubation in each of the PBS standard solutions of IgG or IgM, the gate electrode was washed thoroughly with water (HPLC grade) to remove the unreacted ligands and further I–V transfer curves were measured. All the data points are averaged over three replicates. The resulting reproducibility error is computed as one relative standard deviation.

Supporting Information

Supporting Information is available from the Wiley Online Library or from the author.

Acknowledgements

Conflict of Interest

The authors declare no conflict of interest.

Data Availability Statement

The data that support the findings of this study are available from the corresponding author upon reasonable request.

Keywords

[1] M. Yoshitake, *Work Function and Band Alignment of Electrode Materials*, Springer, Tokio, Japan, https://doi.org/10.1007/978-4-431-56898-8_8.

[2] E. Macchia, K. Manoli, B. Holzer, C. Di Franco, M. Ghittorelli, F. Torricelli, D. Alberga, G. F. Mangiatordi, G. Palazzo, G. Scamarcio, L. Torsi, *Nat. Commun.* **2018**, *9*, 3223.

[3] E. Macchia, F. Torricelli, P. Bollella, L. Sarcina, A. Tricase, C. Di Franco, R. Österbacka, Z. M. Kovács-Vajna, G. Scamarcio, L. Torsi, *Chem. Rev.* **2022**, *122*, 4636.

[4] A. K. Sinensky, A. M. Belcher, *Nat. Nanotechnol.* **2007**, *2*, 653.

[5] M. Nonnenmacher, M. P. O'Boyle, H. K. Wickramasinghe, *Appl. Phys. Lett.* **1991**, *58*, 2921.

[6] K. P. Pernstich, S. Haas, D. Oberhoff, C. Goldmann, D. J. Gundlach, B. Batlogg, A. N. Rashid, G. Schitter, *J. Appl. Phys.* **2004**, *96*, 6431.

[7] S. Kobayashi, T. Nishikawa, T. Takenobu, S. Mori, T. Shimoda, T. Mitani, H. Shimotani, N. Yoshimoto, S. Ogawa, Y. Iwasa, *Nat. Mater.* **2004**, *3*, 317.

[8] L. Kergoat, L. Herlogsson, D. Braga, B. Piro, M. C. Pham, X. Crispin, M. Berggren, G. Horowitz, *Adv. Mater.* **2010**, *22*, 2565.

[9] C. Loppacher, in *Springer Series in Surface Sciences*, (Eds: S. Sadewasser, T. Glatzel) Springer, Berlin **2012**, pp. 221.

[10] A. Liscio, V. Palermo, K. Müllen, P. Samorì, *J. Phys. Chem. C* **2008**, *112*, 17368.

[11] N. Turetta, F. Sedona, A. Liscio, M. Sambi, P. Samorì, *Adv. Mater. Interfaces* **2021**, *8*, 2100068.

[12] B. Holzer, K. Manoli, N. Ditaranto, E. Macchia, A. Tiwari, C. Di Franco, G. Scamarcio, G. Palazzo, L. Torsi, *Adv. Biosyst.* **2017**, *1*, 1700055.

[13] S. Casalini, A. C. Dumitru, F. Leonardi, C. A. Bortolotti, E. T. Herruzo, A. Campana, R. F. De Oliveira, T. Cramer, R. Garcia, F. Biscarini, *ACS Nano* **2015**, *9*, 5051.

[14] E. Macchia, L. De Caro, F. Torricelli, C. Di Franco, C. Di Franco, P. L. Torsi, C. Di Franco, P. G. Scamarcio, *Adv. Sci.* **2022**, *9*, 2104381.

[15] G. Horowitz, P. Lang, M. Mottaghi, H. Aubin, *Adv. Funct. Mater.* **2004**, *14*, 1069.

[16] G. Horowitz, P. Delannoy, *J. Appl. Phys.* **1991**, *70*, 468.

[17] E. Macchia, R. A. Picca, K. Manoli, C. Di Franco, D. Blasi, L. Sarcina, N. Ditaranto, N. Cioffi, R. Österbacka, G. Scamarcio, F. Torricelli, L. Torsi, *Mater. Horiz.* **2020**, *7*, 999.

[18] E. Macchia, K. Manoli, C. Di Franco, R. A. Picca, R. Österbacka, G. Palazzo, F. Torricelli, G. Scamarcio, L. Torsi, *ACS Sens.* **2020**, *5*, 1822.

[19] E. Macchia, L. Sarcina, R. A. Picca, K. Manoli, C. Di Franco, G. Scamarcio, L. Torsi, *Anal. Bioanal. Chem.* **2020**, *412*, 811.

[20] F. Torricelli, D. Z. Adrahtas, F. Biscarini, A. Bonfiglio, C. A. Bortolotti, C. D. Frisbie, I. Mcculloch, E. Macchia, G. G. Malliaras, *Nat. Rev. Methods Primers* **2021**, *1*, 66.

[21] E. Macchia, A. Tiwari, K. Manoli, B. Holzer, N. Ditaranto, R. A. Picca, N. Cioffi, C. Di Franco, G. Scamarcio, G. Palazzo, L. Torsi, *Chem. Mater.* **2019**, *31*, 6476.

[22] E. Macchia, Z. M. Kovács-vajna, D. Loconsole, L. Sarcina, M. Redolfi, M. Chironna, F. Torricelli, L. Torsi, D. Chimica, B. Aldo, *Sci. Adv.* **2022**, *8*, eabo0881.

[23] K. Banerjee-Ghosh, S. Ghosh, H. Mazal, I. Riven, G. Haran, R. Naaman, *J. Am. Chem. Soc.* **2020**, *142*, 20456.

[24] V. K. Gupta, J. J. Skaife, T. B. Dubrovsky, N. L. Abbott, *Science* **1998**, *279*, 2077.

[25] S. Sadewasser, P. Jelinek, C. K. Fang, O. Custance, Y. Yamada, Y. Sugimoto, M. Abe, S. Morita, *Phys. Rev. Lett.* **2009**, *103*, 266103.

[26] D. Blasi, F. Viola, F. Modena, A. Luukkonen, E. MacChia, R. A. Picca, Z. Gounani, A. Tewari, R. Österbacka, M. Caironi, Z. M. Kovacs Vajna, G. Scamarcio, F. Torricelli, L. Torsi, *J. Mater. Chem. C* **2020**, *8*, 15312.